Two pairing domes as Cu^{2+} varies to Cu^{3+}

Thomas Maier, T. Berlijn, and D. J. Scalapino

Phys. Rev. B **99**, 224515 — Published 27 June 2019

DOI: 10.1103/PhysRevB.99.224515

Two pairing domes as Cu^{2+} varies to Cu^{3+}

Thomas Maier,[1,2] T. Berlijn,[1,2] and D.J. Scalapino[3]

[1] *Computational Sciences and Engineering Division, Oak Ridge National Lab, Oak Ridge, Tennessee 37831, USA*
[2] *Center for Nanophase Materials Sciences, Oak Ridge National Laboratory, Oak Ridge, Tennessee 37831, USA*
[3] *Department of Physics, University of California, Santa Barbara, CA 93106-9530, USA*

(Dated: June 6, 2019)

Using a tight-binding two-orbital ($d_{x^2-y^2}$, $d_{3z^2-r^2}$) model and a random phase approximation treatment of the spin-fluctuation pairing vertex, we calculate the pairing strengths for a cuprate model in which the hole doping varies from Cu^{2+} to Cu^{3+}. We find two domes of pairing strength, one corresponding to the traditional low hole doping regime and the other to the extremely overdoped regime discussed by Geballe and Marezio [1]. In the overdoped regime we find that there is significant pairing strength in both the d-wave and $s^{\pm}$ channels.

In 2009, Geballe and Marezio [1] published a review of superconductivity in $Sr_2CuO_{4-\delta}$ [2, 3] in which they noted that, while it was isostructured to the familiar 214 La_2CuO_4 system, it was extremely overdoped and had a superconducting transition temperature of $T_c = 95$ K, which was more than twice that of optimally doped $La_{1.84}Sr_{0.16}CuO_4$. Since that time bulk superconductivity at $T_c = 84$ K in $Cu_{0.75}Mo_{0.25}Sr_2YCu_2O_{7.54}$ [4] and exceeding 70 K in $Ba_2CuO_{4-\delta}$ [5] have been reported. In addition, monolayer CuO_2 films grown on Bi2212 substrates exhibit tunneling gap features suggesting superconductivity up to 100K [6]. All of these materials are characterized as highly overdoped, and the $Ba_2CuO_{4-\delta}$ and $Sr_2CuO_{4-\delta}$ systems have a reduced Cu apical O spacing compared to typical cuprate superconductors. Here, using a two-orbital ($d_{x^2-y^2}$,$d_{3z^2-r^2}$) tight-binding model and a multi-orbital random phase approximation (RPA) calculation [7, 8] of the pairing vertex, we will study the pairing strength as the hole doping $0 < x < 1$ varies from underdoped to highly overdoped and the octahedron CuO_6 structure is compressed.

In the high-pressure oxidized synthesis as the doping x increases and the Cu apical O distance decreases, the energy splitting between the $3d_{x^2-y^2}$ and $3d_{3z^2-r^2}$ orbitals decreases. The phenomenological tight-binding model we will use is derived from a Wannier function based Hamiltonian obtained from a density functional theory (DFT) calculation of a compressed Ba_2CuO_4 compound for $x = 1$ [9–14]. It describes two bands formed from the Cu $3d_{x^2-y^2}$ and $3d_{3z^2-r^2}$ orbitals. As the doping x decreases to zero, the energy splitting $\Delta E(x)$ between the $3d_{x^2-y^2}$ and $3d_{3z^2-r^2}$ orbitals in our model is increased. As illustrated in Fig. 1a at low doping, $x = 0.15$, a single band crosses the Fermi energy. In this case, the Fermi surface in Fig. 3a has a hole-like sheet with majority $d_{x^2-y^2}$ orbital weight around the (π, π) point of the 2D Brillouin zone. For the strongly overdoped high-pressure synthesized material with $x = 0.85$, the bandstructure shown in Fig. 1b has two bands crossing the Fermi energy. In this case, there is an electron-like sheet with $d_{x^2-y^2}$ and $d_{3z^2-r^2}$ orbital weights around the zone center Γ as shown in Fig. 3a and a hole-like sheet around the (π, π) point with dominantly $d_{3z^2-r^2}$ orbital weight as shown in Fig. 4a.

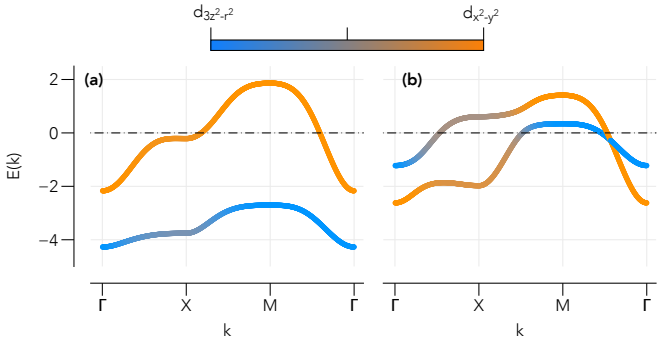

FIG. 1: The two-orbital tight binding bandstructure for Cu^{2+x} dopings of $x = 0.15$ and 0.85. For the underdoped case (a), a single band with dominant $d_{x^2-y^2}$ orbital character crosses the Fermi energy. In the extremely overdoped system (b) with a reduced Cu apical O spacing, two bands with $d_{x^2-y^2}$ and $d_{3z^2-r^2}$ orbital weights cross the Fermi energy. The orbital weights for $d_{x^2-y^2}$ and $d_{3z^2-r^2}$ are indicated by orange and blue, respectively.

The two orbital Hamiltonian we will study has a band structure given by

$$H_0(x) = \sum_{k\sigma} \sum_{\ell\ell'} \left(\xi_{\ell\ell'}(k) + (\varepsilon_\ell(x) - \mu)\,\delta_{\ell\ell'}\right) d^\dagger_{\ell\sigma}(k) d_{\ell'\sigma}(k) \tag{1}$$

Here $\ell = 1$ denotes the $d_{x^2-y^2}$ orbital, $\ell = 2$ the $d_{3z^2-r^2}$ orbital and its energy $\varepsilon_2(x) = \varepsilon_1 - \Delta E(x)$, where $\Delta E(x)$ is a linearly decreasing function of x, given in the Supplementary Material [9] together with the other tight-binding parameters. For the Fermi surfaces shown in Figs. 3a and 4a, the chemical potential μ has been adjusted to give dopings of $x = 0.15$ and 0.85, respectively, corresponding to a filling $\langle n \rangle = 3 - x$. The onsite interaction part of the Hamiltonian has the usual on-site

form

$$H_1 = U\sum_{i,\ell} n_{i\ell\uparrow}n_{i\ell\downarrow} + U'\sum_{i,\ell'<\ell} n_{i\ell}n_{i\ell'} + J\sum_{i,\ell'<\ell\sigma,\sigma'}\sum d^\dagger_{i\ell\sigma}d^\dagger_{i\ell'\sigma'}d_{i\ell\sigma'}d_{i\ell'\sigma} + J'\sum_{i,\ell'\neq\ell} d^\dagger_{i\ell}d^\dagger_{i\ell\downarrow}d_{i\ell'\downarrow}d_{i\ell'\uparrow}. \quad (2)$$

Here, U and U' are the local intra- and inter-orbital Coulomb repulsions, respectively, J is the Hund's rule exchange and J' the pair hopping term. In the following we will use interaction parameters $U = 1.3$, $U' = 1.05$, $J = J' = 0.125$ in units of eV. These parameters satisfy rotational invariance and are chosen so that the maximum pairing strength $\lambda_\alpha \sim 0.5$ in the RPA treatment. There is of course a change in the Coulomb interaction parameters which would be expected to decrease as the doping increases. Here we have chosen to keep them constant in order to compare the effects of the change in the orbital occupation and Fermi surface structure on the size of the pairing strength λ_α. A similar 2-orbital ($d_{x^2-y^2}$, $d_{3z^2-r^2}$) Hamiltonian has been used by Jiang et al. [15] to model a CuO_2 monolayer on Bi2212 [6]. Treating this model using a Gutzwiller approximation, they derived a spin-orbit superexchange pairing interaction of the Kugel-Kohmskii form and find nodeless A_{1g} $s^\pm$ pairing.

In the multi-orbital RPA theory the pairing vertex $\Gamma_{\ell_1\ell_2\ell_3\ell_4}(k,k')$ for scattering a singlet pair $(k\uparrow \ell_1, -k\downarrow \ell_4)$ in orbitals ℓ_1 and ℓ_4 to $(k'\uparrow \ell_2, -k'\downarrow \ell_3)$ in orbitals ℓ_2 and ℓ_3 illustrated in Fig. 2 is given by

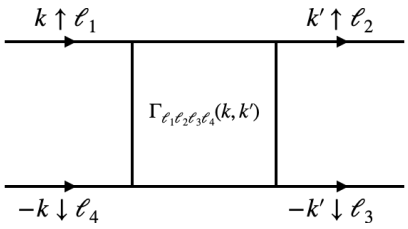

FIG. 2: The vertex for scattering a $(k\uparrow \ell_1, -k\downarrow \ell_4)$ pair to a $(k'\uparrow \ell_2, -k'\downarrow \ell_3)$ pair with $\ell = 1$ for the $d_{x^2-y^2}$ orbit and $\ell = 2$ for the $d_{3z^2-r^2}$ orbit.

$$\Gamma_{\ell_1\ell_2\ell_3\ell_4}(k,k') = \Big[\frac{3}{2}\,U^s\chi_S^{\rm RPA}(k-k')U^s - \frac{1}{2}\,U^c\chi_O^{\rm RPA}(k-k')U^c + \frac{1}{2}\,(U^s+U^c)\Big]_{\ell_1\ell_2\ell_3\ell_4}. \quad (3)$$

Here U^s and U^c represent 4×4 matrices in orbital space which depend on the interaction parameters and $\chi_S^{\rm RPA}$ and $\chi_O^{\rm RPA}$ are orbital matrix RPA spin and orbital (charge) susceptibilities given in the Supplementary Material [9].

The dominant orbital scattering vertices for a doping of $x = 0.15$ are shown in Fig. 3.

Here k is fixed at the bottom of the hole Fermi surface (the point labeled 60) that surrounds the M point and k' varies over the Fermi surface points 0–79 as indicated in Fig. 3a. The dominant contribution to the pairing is associated with the orbital vertex Γ_{1111} in which the electrons are in the $d_{x^2-y^2}$ orbital. The strength of this vertex peaks at momentum transfers $k'-k$ equal to Q_1 and Q_2 shown in Fig. 3a.

As we have seen, for the compressed heavily overdoped material, both the $d_{x^2-y^2}$ and the $d_{3z^2-r^2}$ orbitals are present near the Fermi surfaces with considerable weight associated with the $d_{3z^2-r^2}$ orbital. In this case, as shown in Fig. 4 for a doping $x = 0.85$, the dominant contribution to the pairing is associated with the orbital vertices Γ_{2222}, Γ_{1122}, Γ_{2211} and Γ_{1111}. The Γ_{2222} vertex involves scattering between pairs with $d_{3z^2-r^2}$ orbital weight while the latter Γ_{1111} vertex involves pairs with $d_{x^2-y^2}$ orbital weight. As seen in Fig. 4a, for the shortened Cu apical O distance and $x = 0.85$ doping, the $d_{3z^2-r^2}$ orbital weight is larger than the $d_{x^2-y^2}$ orbital weight over most parts of the Fermi surfaces. The Γ_{1122} and Γ_{2211} vertices involve both the $d_{3z^2-r^2}$ and $d_{x^2-y^2}$ orbitals and have an intermediate strength. The momentum dependence of the vertices reflect the $k'-k$ momentum transfers Q_1, Q_2 and Q_3 indicated in Fig. 4a.

In terms of the scattering vertices, the pairing strength is given by the eigenvalue of

$$-\sum_j \oint \frac{dk'_\parallel}{2\pi v_{F_j}(k'_\parallel)}\Gamma_{ij}(k,k')g_j^\alpha(k') = \lambda_\alpha g_i^\alpha(k) \quad (4)$$

with

$$\Gamma_{ij}(k,k') = \sum_{\ell_1\ell_2\ell_3\ell_4} a^{\ell_1}_{\nu_i}(k)a^{\ell_4}_{\nu_i}(-k)\Gamma_{\ell_1\ell_2\ell_3\ell_4}(k,k') \times a^{\ell_2 *}_{\nu_j}(k')a^{\ell_3 *}_{\nu_j}(-k') \quad (5)$$

Here j sums over the Fermi surfaces, $v_{F_j}(k'_\parallel)$ is the Fermi velocity $|\nabla_k E_{\nu_j}(k)|$ and the integral runs over the Fermi surface or surfaces. We have calculated the leading B_{1g} (d-wave) and A_{1g} ($s^\pm$-wave) pairing strength eigenvalues as a function of the doping x. The results plotted in Fig. 5a show that for the traditional "low-doping" region ($x \sim 0.15$) the pairing strength is in the B_{1g} (d-wave) channel as expected. However, in the strongly overdoped ($x \sim 0.85$) regime both the B_{1g} (d-wave) and A_{1g} ($s^\pm$-wave) pairing strengths are significant and quite close to each other.

As seen in Fig. 4, the dominant pair scattering process with momentum transfer Q_2 contributes to the pairing strength in both the d-wave and the $s^\pm$ channels. Similarly the scattering Q_1 contributes to both, while the

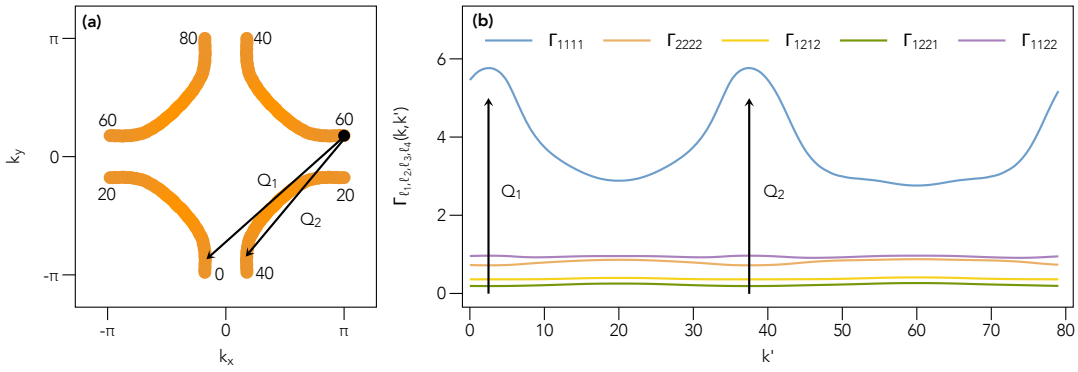

FIG. 3: (a) The Fermi surface for $x = 0.15$ and (b) selected orbital dependent vertices versus k' with k fixed at 60. The dominant orbital weight on the Fermi surface for $x = 0.15$ is $d_{x^2-y^2}$ and the peaks in Γ_{1111} seen in (b) arise from the $k'_1 - k_1$ scattering processes labeled Q_1 and Q_2 in (a).

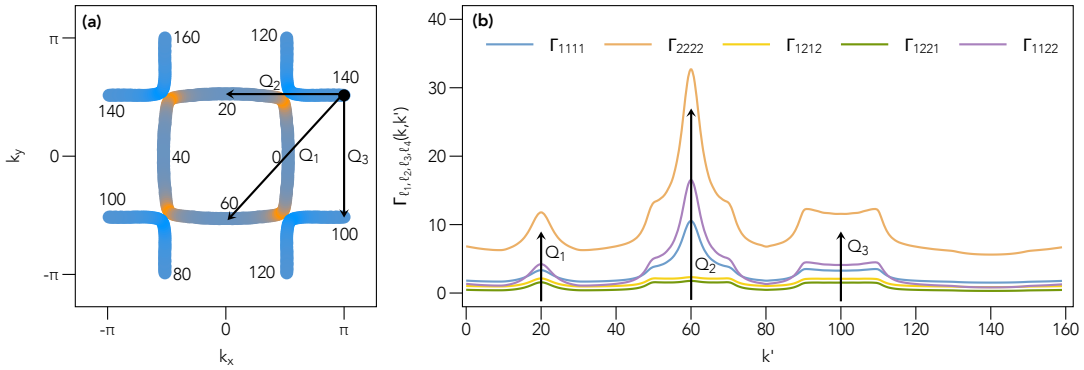

FIG. 4: (a) The Fermi surface for $x = 0.85$ and (b) selected orbital dependent vertices versus k' with k fixed at 140. In this case, there is significant $d_{3z^2-r^2}$ orbital weight on the Fermi surface. The structure in the vertices arises from the scattering processes indicated in (a).

scattering at Q_3 contributes negatively. These same momentum transfers are effective in scattering electron pairs between the corners of the electron and of the hole Fermi surfaces. These processes lead to the "accidental" nodes of the $s^{\pm}$ gap function.

To conclude, for the two-orbital ($d_{x^2-y^2}$, $d_{3z^2-r^2}$) RPA model we have studied we find two T_c domes, one in the underdoped and one in the highly overdoped regime. As expected, in the low doping region there is B_{1g} (d-wave) pairing. In the extremely overdoped $x \approx 0.85$ region we find pairing strength in both the B_{1g} (d-wave) and A_{1g} ($s^{\pm}$-wave) channels. The pairing strength in this second region is larger relative to that found in the small doping region and that for an optimally doped single-band Hubbard model. This is in spite of the two orbitals $d_{x^2-y^2}$ and $d_{3z^2-r^2}$ each having significant orbital weight at the Fermi energy. This appears counter to previous calculations which concluded that T_c is optimized when the orbital weight is concentrated in a single $d_{x^2-y^2}$ orbital [16, 17]. However, similar spin-fluctuation based pairing calculations [18] have found that T_c is enhanced in systems which have both electron- and hole-Fermi surfaces. This enhancement has also been seen in DCA calculations for a 2-layer Hubbard model with electron and hole bands [19]. We believe that having both electron- and hole-Fermi surfaces is sufficiently advantageous that it overcomes the orbital weight effect and is responsible for the second superconducting dome in the highly overdoped region of the cuprate phase diagram proposed by Geballe and Marezio [1]. The occurance of two pairing channels in this overdoped cuprate regime is reminiscent of $Ba_{0.6}K_{0.4}Fe_2As_2$. In that case, below T_c an emergent B_{1g} (d-wave) mode is observed in Raman scattering [20]. This has been interpreted as arising from a Bardasis-Schrieffer mode associated with a subdominant $d_{x^2-y^2}$ pairing channel in an $s^{\pm}$ superconductor. In the present case, in the second dome one could have a d-wave superconductor with a close lying subdominant $s^{\pm}$ mode. The Raman observation of such behavior would provide an interesting link between the cuprate and Fe-based superconductors.

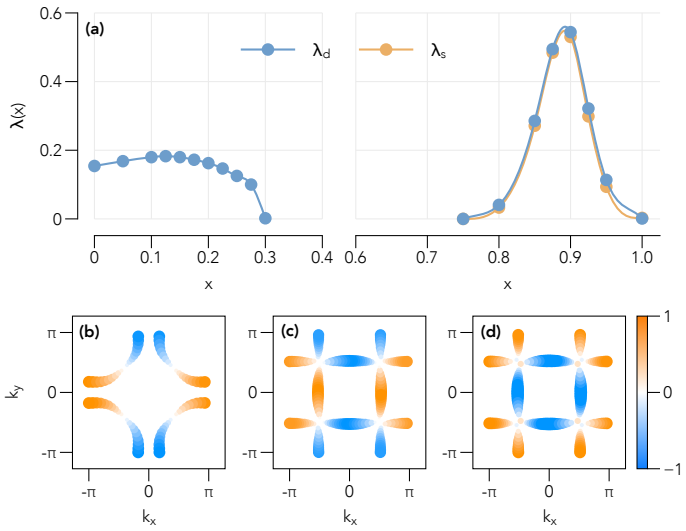

FIG. 5: (a) The pairing strength eigenvalue $\lambda_\alpha(x)$ versus doping for $s^\pm$ and $d_{x^2-y^2}$ pairing shows two domes, one in the underdoped and another in the highly over doped regime. (b) The gap function for the leading $d_{x^2-y^2}$ eigenvalue for $x = 0.15$. (c) The $d_{x^2-y^2}$ gap function for $x = 0.80$ and (d) the $s^\pm$ gap function for $x = 0.85$.

Acknowledgments

The possibility of another region of superconductivity in the extremely overdoped cuprates was proposed to one of us by Theodore H. Geballe a number of years ago. We thank S. Uchida for discussions regarding the structure of the oxygen efficient 214 cuprates. The DFT calculations, the derivation of the tight-binding model (TB) and the analysis of the results (DJS) were supported by the Scientific Discovery through Advanced Computing (SciDAC) program funded by U.S. Department of Energy, Office of Science, Advanced Scientific Computing Research and Basic Energy Sciences, Division of Materials Sciences and Engineering. The RPA calculations (TAM) were supported by the U.S. Department of Energy, Office of Basic Energy Sciences, Materials Sciences and Engineering Division.

[1] T. H. Geballe, M. Marezio, *Physica C* **469**, 680 (2009).
[2] Q. Q. Liu, H. Yang, X. M. Qin, Y. Yu, L. X. Yang, F. Y. Li, R. C. Yu, C. Q. Jin, and S. Uchida, *Phys. Rev. B* **74**, 100506 (2006).
[3] Z. Hiroi, M. Takano, M. Azuma, Y. Takeda, *Nature* **364**, 315 (1993).
[4] A. Gauzzi, Y. Klein, M. Nisula, M. Karppinen, P. K. Biswas, H. Saadaoui, E. Morenzoni, P. Manuel, D.Khalyavin, M. Marezio, and T. H. Geballe, *Phys. Rev. B* **94**, 180509 (R) (2016).
[5] W. M. Li, L. P. Cao, J. F. Zhao, R. Z. Yu, J. Zhang, Y. Liu, Q. Q. Liu, G. Q. Zhao, X. C. Wang, Z. Hu, Q. Z. Huang, H. Wu, H. J. Lin, C. T. Chen, J. S. Kim, G. Steward, Z. Li, Y. W. Long, Z. Z. Gong, Z. Guguchia, Y. J. Uemura, S. Uchida, C. Q Jin, preprint arXiv:1808.09425 (2018).
[6] Y. Zhong, Y. Wang, S. Han, Y.-F. Lv, W.-L. Wang, D. Zhang, H. Ding, Y.-M. Zhang, L. Wang, K. He, R. Zhong, J. A. Schneeloch, G.-D. Gu, C.-L. Song, X.-C. Ma, Q.-K. Xue, *Science Bulletin* **61**, 1239 (2016).
[7] K. Kubo, *Phys. Rev. B* **75**, 224509 (2007).
[8] A. F. Kemper, T. A. Maier, S. Graser, P. J. Hirschfeld, D. J. Scalapino, *New J. Phys.* **12**, 073030 (2010).
[9] See Supplemental Material at [URL will be inserted by publisher] for more details on the DFT bandstructure calculation, the tight-binding Hamiltonian and the RPA calculation and results.
[10] K. Schwarz, P. Blaha, G. K. H. Madsen, Comput. Phys. Commun. **147**, 71 (2002).
[11] J. P. Perdew, K. Burke and M. Ernzerhof, Phys. Rev. Lett. **77**, 3865 (1996).
[12] W. M. Li, L. P. Cao, J. F. Zhao, R. Z. Yu, J. Zhang, Y. Liu, Q. Q. Liu, G. Q. Zhao, X. C. Wang, Z. Hu, Q. Z. Huang, H. Wu, H. J. Lin, C. T. Chen, J. S. Kim, G. Steward, Z. Li, Y. W. Long, Z. Z. Gong, Z. Guguchia, Y. J. Uemura. S. Uchida, C. Q Jin, preprint arxiv:1808.09425 (2018).
[13] J. Kunes, R. Arita, P. Wissgott, A. Toschi, H. Ikeda, and K. Held, Comp. Phys. Commun. **181**, 1888 (2010).
[14] A. A. Mostofi, J. R. Yates, G. Pizzi, Y. S. Lee, I. Souza, D. Vanderbilt and N. Marzari Comput. Phys. Commun. **185**, 2309 (2014).
[15] K. Jiang, X. Wu, J. Hu and Z. Wang, Phys. Rev. Lett. 121, 227002 (2018).
[16] E. Pavarini, I. Dasgupta, T. Saha-Dasgupta, O. Jepsen, O. K. Anderson, *Phys. Rev. Lett.* **87**, 047003 (2001).
[17] H. Sakakibara, K. Suzuki, H. Usui, K. Kuroki, R. Arita, D. J. Scalapino, H. Aoki, *Physics Procedia* **45**, 13 (2013).
[18] M. Nakata, D. Ogura, H. Usui, K. Kuroki, *Phys. Rev. B* **95**, 214509 (2017)
[19] T. Maier and D.J. Scalapino, *Phys. Rev. B* **84**, 180513(R) (2011).
[20] T. Bohm, A. F. Kemper, B. Moritz, F. Kretzschmar, B. Muschler, H.-M. Eiter, R. Hackl, T. P. Devereaux, D.J. Scalapino, and H.-H. Wen, *Phys. Rev. X* **4**, 041046 (2014)